responses may differ when different anesthetics are used or when the animals are in a conscious state. However, as we compared the effects of gadolinium on the reflex responses to MA and EA under the same anesthetic conditions, the interpretation of the sensory mechanisms for MA and EA should be valid. Second, we performed EA at frequencies of 10 or 20 Hz in order to obtain AP and HR responses comparable to those observed during MA under control conditions. Because the effects of EA may differ depending on the magnitude of stimulation including pulse duration, current and frequency (Uchida et al., 2008; Kawada et al., 2009), further studies are needed to examine whether the effects of gadolinium on EA-induced hemodynamic responses vary depending on the stimulation intensities.

4.5. Conclusion

Intravenous administration of gadolinium attenuated the AP and HR responses to both MA and EA, suggesting that the mechanosensitive ion channels are involved in the sensory mechanisms of both MA and EA. EA may cause electrical twitching of surrounding tissues and induce MA-like stimulation through mechanoreceptors.

Acknowledgments

This study was supported by Health and Labour Sciences Research Grants (H19-nano-Ippan-009, H20-katsudo-Shitei-007, and H21-nano-Ippan-005) from the Ministry of Health, Labour and Welfare of Japan; by a Grant-in-Aid for Scientific Research (No. 20390462) from the Ministry of Education, Culture, Sports, Science and Technology of Japan; and by the Industrial Technology Research Grant Program from the New Energy and Industrial Technology Development Organization (NEDO) of Japan.

Appendix A

In an attempt to demonstrate that gadolinium does not significantly affect the hemodynamic responses to direct nerve stimulation related to acupuncture at the hind limb, we performed an additional protocol of tibial nerve stimulation in 5 anesthetized rats. The right tibial nerve was exposed and placed on a pair of platinum electrodes, and was stimulated for 120 s (500 μs, 10 Hz, 2 or 5 mA). ΔAP was -10.5 ± 3.5 mm Hg under baseline conditions, which was attenuated to -8.2 ± 4.4 mm Hg after gadolinium administration ($74 \pm 15\%$ of the pre-gadolinium, $P<0.01$). Although the relative reduction seemed smaller than that observed in EA ($38 \pm 11\%$ of the pre-gadolinium, see main text), because the reduction of ΔAP could be partly attributable to the decreased baseline AP after gadolinium administration, we could not judge whether gadolinium had truly inhibited the hypotensive effect of tibial nerve stimulation. Unfortunately, the tibial nerve stimulation did not change HR significantly in our experimental conditions ($\Delta HR = -1.1 \pm 4.4$ bpm before gadolinium vs. $\Delta HR = -1.4 \pm 4.1$ bpm after gadolinium), as opposed to a previous study (Uchida et al., 2008). As a result, we could not judge the effect of gadolinium based on HR either. We think the ADN stimulation protocol in the main text would be a second best surrogate to indicate the inability of gadolinium to block hemodynamic responses induced by direct activation of the afferent nerve.

References

Adding, L.C., Bannenberg, G.L., Gustafsson, L.E., 2001. Basic experimental studies and clinical aspects of gadolinium salts and chelates. Cardiovasc. Drug Rev. 19, 41–56.
Aplin, A.E., Howe, A., Alahari, S.K., Juliano, R.L., 1998. Signal transduction and signal modulation by cell adhesion receptors: the role of integrins, cadherins, immunoglobulin-cell adhesion molecules, and selectins. Pharmacol. Rev. 50 (2), 197–263.
Burnstock, G., 2009. Acupuncture: a novel hypothesis for the involvement of purinergic signalling. Med. Hypotheses 73, 470–472.
Cho, H., Shin, J., Shin, C.Y., Lee, S., Oh, U., 2002. Mechanosensitive ion channels in cultured sensory neurons of neonatal rats. J. Neurosci. 22 (4), 1238–1247.
Glantz, S.A., 2002. Primer of Biostatistics, 5th ed. McGraw-Hill, New York.
Gschossmann, J.M., Chaban, V.V., McRoberts, J.A., Raybould, H.E., Young, S.H., Ennes, H.S., Lembo, T., Mayer, E.A., 2000. Mechanical action of dorsal root ganglion cells in vitro: comparison with capsaicin and modulation by kappa-opioids. Brain Res. 856 (1–2), 101–110.
Kawada, T., Shimizu, S., Yamamoto, T., Shishido, T., Kamiya, A., Miyamoto, T., Sunagawa, K., Sugimachi, M., 2009. Servo-controlled hind-limb electrical stimulation for short-term arterial pressure control. Circ. J. 73 (5), 851–859.
Kimura, A., Sato, A., 1997. Somatic regulation of autonomic functions in anesthetized animals—neural mechanisms of physical therapy including acupuncture. Jpn J. Vet. Res. 45 (3), 137–145.
Langevin, H.M., Churchill, D.L., Cipolla, M.J., 2001. Mechanical signaling through connective tissue: a mechanism for the therapeutic effect of acupuncture. FASEB J. 15, 2275–2285.
Lin, M.C., Nahin, R., Gershwin, M.E., Longhurst, J.C., Wu, K.K., 2001. State of complementary and alternative medicine in cardiovascular, lung, and blood research: executive summary of a workshop. Circulation 103 (16), 2038–2041.
Nakamoto, T., Matsukawa, K., 2007. Muscle mechanosensitive receptors close to the myotendinous junction of the Achilles tendon elicit a pressor reflex. J. Appl. Physiol. 102, 2112–2120.
Napadow, V., Makris, N., Liu, J., Kettner, N.W., Kenneth, K.K., Hui, K.K.S., 2005. Effects of electroacupuncture versus manual acupuncture on the human brain as measured by fMRI. Hum. Brain Mapp. 24, 193–205.
Sato, A., Sato, Y., Schmidt, R.F., 1981. Heart rate changes reflecting modifications of efferent cardiac sympathetic outflow by cutaneous and muscle afferent volleys. J. Auton. Nerv. Syst. 4 (3), 231–247.
Sato, A., Sato, Y., Suzuki, A., Uchida, S., 1994. Reflex modulation of gastric and vesical function by acupuncture-like stimulation in anesthetized rats. Biomed. Res. 15, 59–65.
Sato, A., Sato, Y., Uchida, S., 2002. Reflex modulation of visceral functions by acupuncture-like stimulation in anesthetized rats. Int. Congr. Ser. 1238, 111–123.
Sator-Katzenschlager, S.M., Szeles, J.C., Scharbert, G., Michalek-Sauberer, A., Kober, A., Heinze, G., Kozek-Langenecker, S.A., 2003. Electrical stimulation of auricular acupuncture points is more effective than conventional manual auricular acupuncture in chronic cervical pain: a pilot study. Anesth. Analg. 97, 1469–1473.
Silberstein, M., 2009. The cutaneous intrinsic visceral afferent nervous system: a new model for acupuncture analgesia. J. Theor. Biol. 261, 637–642.
Tjen-A-Looi, S.C., Fu, L.-W., Zhou, W., Syuu, Z., Longhurst, J.C., 2005. Role of unmyelinated fibers in electroacupuncture cardiovascular responses. Auton. Neurosci. 118, 43–50.
Uchida, S., Shimura, M., Ohsawa, H., Suzuki, A., 2007. Neural mechanism of bradycardic responses elicited by acupuncture-like stimulation to a hind limb in anesthetized rats. J. Physiol. Sci. 57 (6), 377–382.
Uchida, S., Kagitani, F., Hotta, H., 2008. Mechanism of the reflex inhibition of heart rate elicited by acupuncture-like stimulation in anesthetized rats. Auton. Neurosci. 143, 12–19.
Wessberg, J., Olausson, H., Fernstrom, W.F., Vallbo, B.A., 2003. Receptive field properties of unmyelinated tactile afferents in the human skin. J. Neurophysiol. 89, 1567–1575.
Yamamoto, H., Kawada, T., Kamiya, A., Kita, T., Sugimachi, M., 2008. Electroacupuncture changes the relationship between cardiac and renal sympathetic nerve activities in anesthetized cats. Auton. Neurosci. 144 (1–2), 43–49.

Please cite this article as: Yamamoto, H., et al., Involvement of the mechanoreceptors in the sensory mechanisms of manual and electrical acupuncture, Auton. Neurosci. (2010), doi:10.1016/j.autneu.2010.11.004

Am J Physiol Regul Integr Comp Physiol 300: R969–R977, 2011.
First published January 26, 2011; doi:10.1152/ajpregu.00768.2010.

Exercise training augments the dynamic heart rate response to vagal but not sympathetic stimulation in rats

Masaki Mizuno,[1,2] Toru Kawada,[2] Atsunori Kamiya,[2] Tadayoshi Miyamoto,[2,3] Shuji Shimizu,[2] Toshiaki Shishido,[2] Scott A. Smith,[1] and Masaru Sugimachi[2]

[1]*Departments of Physical Therapy and Internal Medicine, University of Texas Southwestern Medical Center at Dallas, Dallas, Texas;* [2]*Department of Cardiovascular Dynamics, National Cerebral and Cardiovascular Center Research Institute, Osaka, Japan; and* [3]*Department of Physical Therapy, Morinomiya University of Medical Sciences, Osaka, Japan*

Submitted 23 November 2010; accepted in final form 26 January 2011

Mizuno M, Kawada T, Kamiya A, Miyamoto T, Shimizu S, Shishido T, Smith SA, Sugimachi M. Exercise training augments the dynamic heart rate response to vagal but not sympathetic stimulation in rats. *Am J Physiol Regul Integr Comp Physiol* 300: R969–R977, 2011. First published January 26, 2011; doi:10.1152/ajpregu.00768.2010.—We examined the transfer function of autonomic heart rate (HR) control in anesthetized sedentary and exercise-trained (16 wk, treadmill for 1 h, 5 times/wk at 15 m/min and 15-degree grade) rats for comparison to HR variability assessed in the conscious resting state. The transfer function from sympathetic stimulation to HR response was similar between groups (gain, 4.2 ± 1.5 vs. 4.5 ± 1.5 beats·min^{-1}·Hz^{-1}; natural frequency, 0.07 ± 0.01 vs. 0.08 ± 0.01 Hz; damping coefficient, 1.96 ± 0.55 vs. 1.69 ± 0.15; and lag time, 0.7 ± 0.1 vs. 0.6 ± 0.1 s; sedentary vs. exercise trained, respectively, means ± SD). The transfer gain from vagal stimulation to HR response was 6.1 ± 3.0 in the sedentary and 9.7 ± 5.1 beats·min^{-1}·Hz^{-1} in the exercise-trained group ($P = 0.06$). The corner frequency (0.11 ± 0.05 vs. 0.17 ± 0.09 Hz) and lag time (0.1 ± 0.1 vs. 0.2 ± 0.1 s) did not differ between groups. When the sympathetic transfer gain was averaged for very-low-frequency and low-frequency bands, no significant group effect was observed. In contrast, when the vagal transfer gain was averaged for very-low-frequency, low-frequency, and high-frequency bands, exercise training produced a significant group effect ($P < 0.05$ by two-way, repeated-measures ANOVA). These findings suggest that, in the frequency domain, exercise training augments the dynamic HR response to vagal stimulation but not sympathetic stimulation, regardless of the frequency bands.

heart rate variability; transfer function; systems analysis

HEART RATE VARIABILITY (HRV) is considered to be a useful noninvasive assessment of autonomic nervous system activity. It has been well recognized that exercise training increases HRV at rest (4, 19). A recent meta-analysis by Sandercock et al. (28) demonstrated that exercise training results in significant increases in R-R interval and high-frequency (HF) power of HRV. Nevertheless, not all studies have demonstrated increases in HRV after exercise training (7). To date, the exact mechanisms underlying increases in HRV after exercise training remain to be elucidated. Many earlier studies have suggested that the augmentation of HRV induced by exercise training may be caused by a withdrawal of sympathetic tonus and/or an increase in vagal tonus (5, 14, 36). Autonomic tone assessed by HRV may reflect both the autonomic outflow from the central nervous system and the peripheral autonomic regulation of atrial pacemaker cells. The latter can be assessed quantitatively by examining the heart rate (HR) response to electrical stimulation of the autonomic nerves. Furthermore, recent studies suggested that peripheral autonomic regulation of atrial pacemaker cells could contribute to the exercise training-induced increases in cardiac vagal function (9, 10).

Equivocal results, however, have been reported using autonomic nerve stimulation. Regarding the vagal system, the effects of exercise training have been inconsistent among studies, showing both increases (9, 10) and reductions in vagally stimulated HR control (25). When considering the sympathetic system, a previous study demonstrated that the HR response to sympathetic stimulation was reduced by exercise training (22). However, the mechanisms underlying the training effect are controversial (3, 15, 26, 29, 33, 35). These equivocal results could be explained by differences in species and modes of exercise training among studies (i.e., exercise type, intensity, and duration, etc.). More importantly, since these studies of autonomic nerve stimulation did not evaluate HRV, a causal relationship between increased HRV and adaptation in peripheral autonomic HR control remains largely undetermined. Furthermore, despite the fact that HRV has been evaluated by using frequency domain as well as time domain analyses, to date, there are no reports available examining the effects of exercise training on the dynamic HR response to sympathetic or vagal stimulation in the frequency domain. Analysis of peripheral autonomic regulation in the frequency domain would advance our understanding of the mechanisms responsible for the alterations in HRV that occur in response to exercise training.

We have recently developed a technique to assess the dynamic characteristics of HR control by the autonomic nervous system in rats using transfer function analysis (21). The transfer function analysis can quantitatively evaluate the HR response to autonomic nerve stimulation over a wide frequency range that is necessary for interpreting the generation of HRV. Therefore, the aims of the present study were *1*) to identify the dynamic characteristics of sympathetic and vagal HR control in exercised-trained rats and *2*) to determine whether alterations in peripheral autonomic regulation contribute to changes in the frequency components of HRV in exercised-trained rats.

MATERIALS AND METHODS

Animal Care and Training Program

Animal care was in accordance with the "Guiding Principles for Care and Use of Animals in the Field of Physiological Sciences," approved by the Physiological Society of Japan. All protocols were reviewed and approved by the Animal Subjects Committee of the

Address for reprint requests and other correspondence: M. Mizuno, Dept. of Physical Therapy, Univ. of Texas Southwestern Medical Center at Dallas, 5323 Harry Hines Blvd., Dallas, TX 75390-9174 (e-mail: masaki.mizuno@utsouthwestern.edu).

National Cerebral and Cardiovascular Center. Fourteen male Sprague-Dawley rats (200–250 g body wt) were fed standard laboratory chow and water ad libitum and housed three per cage in a temperature-controlled room with a 12:12-h dark-light cycle. Rats were randomly assigned to one of two groups: sedentary ($n = 7$) and exercise trained ($n = 7$).

Exercise training was performed on a motor-driven treadmill, 5 days/wk for 16 wk, gradually progressing toward a speed of 15 m/min at a 15-degree grade for 60 min. Sedentary rats walked (10 m/min at 15 degrees) 10 min/day once per week during the 16-wk period to maintain treadmill familiarity. At the end of the 16-wk period, maximal exercise capacity was measured twice in each rat in tests separated by 2 days (6). The protocol for the maximal exercise capacity test consisted of walking at 10 m/min for 5 min followed by 2 m/min increases in speed every 2 min until the rat reached exhaustion. Rats were considered exhausted when they failed to stay off of a shock bar.

Assessment of Autonomic Tone in the Conscious Resting State

After the performance test, three steel electrodes were implanted under anesthesia. These electrodes were utilized for monitoring the electrocardiogram. The R-R interval was measured using a cardiotachometer (model AT601G; Nihon Kohden, Tokyo, Japan). On the first day of the study, which was 24 h after electrodes had been implanted, resting HR was recorded to analyze the R-R interval variability in the quiet unrestrained rat that was kept in a small box. In accordance with a previous study (25), autonomic tone was assessed by intraperitoneal injections of methylatropine (3 mg/kg) and propranolol (4 mg/kg). Immediately after resting HR was recorded, methylatropine was injected. Since the HR response to methylatropine reached its peak in 10–15 min, this time interval was allocated before the HR measurement. Propranolol was injected after methylatropine injection, and again the HR was measured after 10–15 min. Intrinsic HR was evaluated after simultaneous blockade by propranolol and methylatropine. Sympathetic tonus was defined as the difference between the HR after methylatropine injection and intrinsic HR. On the second day, propranolol was administered first to obtain the inverse sequence of blockade. Vagal tonus was defined as the difference between the HR after propranolol injection and intrinsic HR.

Sympathetic and Vagal Stimulation

Surgical preparations. After obtaining data for the assessment of autonomic tone and HRV, rats were anesthetized by a mixture of urethane (250 mg/ml) and α-chloralose (40 mg/ml), initiated with an intraperitoneal bolus injection of 1 ml/kg. If additional anesthesia was needed, 0.1 ml/kg was given intraperitoneally. The rats were intubated and mechanically ventilated with oxygen-enriched room air. The rats were slightly hyperventilated to suppress chemoreflexes. A catheter was placed in the right femoral artery and connected to a pressure transducer (model DX-200; Nihon Kohden, Tokyo, Japan) to measure arterial pressure (AP). HR was measured using a cardiotachometer (model AT601G; Nihon Kohden) triggered by the R wave on the electrocardiogram. A catheter was introduced into the right femoral vein for drug administration. Sinoaortic barodenervation was performed bilaterally to minimize changes in sympathetic efferent nerve activity via arterial baroreflexes. The vagi were sectioned bilaterally at the neck. A pair of bipolar stainless steel electrodes was attached to the right cervical sympathetic nerve for efferent sympathetic stimulation or the right cervical vagus for efferent vagal stimulation. The stimulation electrodes and nerve were secured with silicon glue (Kwik-Sil; World Precision Instruments, Sarasota, FL). Body temperature was monitored with a thermometer placed in the rectum and was maintained at 38°C with a heating pad throughout the experiment.

Experimental procedures. The pulse duration was set at 2 ms and the stimulation amplitude was fixed at 10 V for both sympathetic and vagal nerve stimulation. To allow for stabilization of hemodynamics, sympathetic and vagal nerve stimulations were started ~1 h after the end of surgical preparations. Between sympathetic and vagal stimulation protocols > 15 min elapsed to allow AP and HR to return to their respective baseline values.

To estimate the dynamic transfer characteristics from sympathetic stimulation to HR response, the sectioned end of the right cervical sympathetic nerve was stimulated employing a frequency-modulated pulse train for 10 min. The stimulation frequency was switched every 1,000 ms to either 0 or 5 Hz according to a binary white noise signal. The power spectrum of the stimulation signal was reasonably constant up to 0.5 Hz. The transfer function was estimated up to 0.5 Hz because the reliability of estimation decreased due to the diminution of input power above this frequency. The selected frequency range sufficiently spanned the range of physiological interest (21). For estimation of the static transfer characteristics from sympathetic stimulation to HR response, stepwise sympathetic stimulation was performed. Sympathetic stimulation frequency was increased from 1 to 5 Hz in 1-Hz increments. Each frequency step was maintained for 60 s.

To estimate the dynamic transfer characteristics from vagal stimulation to HR response, the right vagus was stimulated employing a frequency-modulated pulse train for 10 min. The stimulation frequency was switched every 500 ms to either 0 or 10 Hz according to a binary white noise signal. The power spectrum of the stimulation signal was reasonably constant up to 1 Hz. The transfer function was estimated up to 1 Hz because the reliability of estimation decreased due to the diminution of input power above this frequency. The selected frequency range sufficiently spanned the range of physiological interest (21). For estimation of the static transfer characteristics from vagal stimulation to HR response, stepwise vagal stimulation was performed. Vagal stimulation frequency was changed among 2, 4, 8, 16, and 32 Hz. Each frequency step was maintained for 60 s.

Data Analysis

Spectral analysis of HRV. Data obtained during the conscious resting state were digitized at 200 Hz utilizing a 12-bit analog-to-digital converter and stored on the hard disk of a dedicated laboratory computer system. Beat-by-beat time series of the R-R interval were interpolated every 130 ms (Δt). Twelve data segments of 512 (N) points overlapping half of the preceding data were processed. For each data segment, after the linear trend was removed and the Hanning window applied, power spectral density was computed using the fast Fourier transform algorithm. The frequency resolution was $\Delta f = 1/(N\,\Delta t)$, i.e., 0.015 Hz, and the highest frequency was $\Delta f = 1/2\Delta t$, i.e., 3.85 Hz, where f is frequency. The very-low-frequency (VLF) band ranged between 0.017 and 0.27 Hz, the low-frequency (LF) band between 0.27 and 0.75 Hz, and the high-frequency (HF) band between 0.75 and 3.3 Hz, according to an earlier report (8). The percentage of LF or HF power relative to the sum of LF and HF powers and the ratio of LF to HF power were also calculated.

Transfer function analysis. The dynamic characteristics of the HR response to sympathetic or vagal stimulation were estimated by a transfer function analysis (see APPENDIX for details). Dynamic sympathetic control of HR was quantified by fitting a second-order low-pass filter with pure delay to the estimated transfer function. The dynamic vagal control of HR was quantified by fitting a first-order, low-pass filter with pure delay to the estimated transfer function. To facilitate the intuitive understanding of the system's dynamic characteristics, we calculated the system step response of HR to 1-Hz nerve stimulation as follows.

The system impulse response was derived from the inverse Fourier transform of the transfer function. The system step response was then obtained from the time integral of the impulse response. The length of the step response was 51.2 s. The 80% rise time for the sympathetic step response or the 80% fall time for the vagal step response was estimated as the time at which the step response reached 80% of the

Table 1. *Physical characteristics*

	Sedentary	Exercise Trained
Body weight, g	642 ± 33	534 ± 33*
Ventricular weight, g	1.22 ± 0.03	1.17 ± 0.04*
Ventricular weight/body weight, g/kg	1.9 ± 0.1	2.2 ± 0.1*
Lung weight, g	2.13 ± 0.27	1.89 ± 0.38
Lung weight/body weight, g/kg	3.3 ± 0.3	3.5 ± 0.7
Performance test, s	1150 ± 165	1790 ± 389*

Values are means ± SD. *$P < 0.05$ compared with sedentary group.

steady-state response calculated by averaging the last 10 s of data of the step response.

Statistical Analysis

All data are represented as means ± SD. Data were analyzed using unpaired Student's *t*-tests (sedentary vs. exercise trained) or two-way, repeated-measures ANOVA. Values of $P < 0.05$ were considered to be significant.

RESULTS

Physical Characteristic

Morphometric characteristics and exercise capacity for sedentary and exercised-trained rats are presented in Table 1. The mean body weight of the exercised-trained rats was significantly smaller than that of the sedentary rats. The mean ventricular weight of the exercised-trained rats was slightly but significantly smaller than that of the sedentary rats. Consequently, the ventricular weight normalized by body weight was significantly greater in the exercised-trained compared with the sedentary group. The lung weight-to-body weight ratio was not different between the groups. Exercise capacity was 64% greater in the exercised-trained than in the sedentary group. The reproducibility of measuring the maximal exercise capacity was reasonably high ($y = 1.2x - 226.1$, $R^2 = 0.79$; x and y represent the first and second measurements).

Spectral Analysis of HRV and Autonomic Tone in the Conscious Resting State

The power spectral densities of R-R interval are shown in Table 2. The percentage of LF power was significantly smaller, and the percentage of HF power was significantly greater in the exercised-trained rats than in the sedentary rats. The LF/HF ratio in the exercised-trained rats was significantly smaller compared with that in the sedentary rats. HR at rest was significantly lower in the exercised-trained compared with the sedentary group (Fig. 1*A*). The intrinsic HR was similar between the groups (Fig. 1*A*). Although the sympathetic tonus was comparable between the groups, the vagal tonus tended to be greater ($P = 0.08$) in the exercised-trained compared with the sedentary group (Fig. 1*B*).

Dynamic Sympathetic and Vagal Transfer Functions

Table 3 summarizes hemodynamics during dynamic sympathetic stimulation. Sympathetic stimulation significantly increased mean HR in both sedentary and exercised-trained groups. Mean HR and AP did not differ between the groups, before and during sympathetic stimulation. Figure 2*A* illustrates the dynamic transfer function characterizing sympathetic HR control. The frequency band effect was significant ($P < 0.0001$) but the group effect was insignificant ($P = 0.5461$) in the dynamic gain values of the sympathetic transfer function by two-way, repeated-measures ANOVA. The parameters of the sympathetic transfer function were comparable between the groups (Table 4). Figure 2*B* shows the calculated step response of HR to sympathetic stimulation. The steady-state response and the 80% rise time did not differ significantly between the groups (Table 4).

Table 5 summarizes hemodynamics during dynamic vagal stimulation. Vagal stimulation significantly decreased mean HR in both sedentary and exercised-trained groups. Mean HR and AP did not differ between the groups, before and during vagal stimulation. Figure 3*A* illustrates the dynamic transfer function characterizing vagal HR control. The frequency band effect ($P < 0.0001$) and the group effect ($P < 0.0001$) were both significant in the dynamic gain values of the vagal transfer function by two-way, repeated-measures ANOVA. The estimated dynamic gain (*see* APPENDIX) tended to be greater in the exercised-trained compared with the sedentary group ($P = 0.06$, Table 6). Other parameters did not differ between the groups. Figure 3*B* shows the calculated step response of HR to vagal stimulation. The calculated steady-state response in the exercised-trained rats also tended to be greater than that in the sedentary rats ($P = 0.06$, Table 6). There was no significant difference in the 80% fall time between the groups.

Dynamic Gain Values of Sympathetic and Vagal Transfer Function Corresponding to HRV Frequency Bands

When dynamic gain values of the sympathetic transfer function were averaged for the VLF and LF (up to 0.5 Hz, see METHODS) bands, the frequency band effect was significant, but the group effect was insignificant by two-way, repeated-measures ANOVA (Fig. 4*A*). When dynamic gain values of the vagal transfer function were averaged for the VLF, LF, and HF (up to 1 Hz, see METHODS) bands, the frequency band effect was insignificant but the group effect was significant such that the dynamic gain was significantly greater in the exercised-trained compared with the sedentary group (Fig. 4*B*).

Static Sympathetic and Vagal Transfer Function

The increase in HR with stepwise sympathetic stimulation was similar between groups (Fig. 5*A*). The stimulation frequency effect was significant, while the group effect was insignificant by two-way, repeated-measures ANOVA. In contrast, the decrease in HR with stepwise vagal stimulation was greater in the exercised-trained compared with sedentary rats (Fig. 5*B*). Both the stimulation frequency effect and the group effect were significant.

Table 2. *Spectral parameters of R-R interval*

	Sedentary	Exercise Trained
Variance, ms^2	87 ± 39	90 ± 32
VLF, ms^2	73 ± 30	80 ± 30
LF, ms^2	6.3 ± 3.4	3.1 ± 3.0
LF, %	49 ± 11	36 ± 7*
HF, ms^2	8.0 ± 7.6	6.2 ± 7.1
HF, %	51 ± 11	64 ± 7*
LF/HF ratio	1.0 ± 0.5	0.6 ± 0.2*

Values are means ± SD. LF, low frequency; VLF, very low frequency; HF, high frequency; *$P < 0.05$ compared with sedentary group.

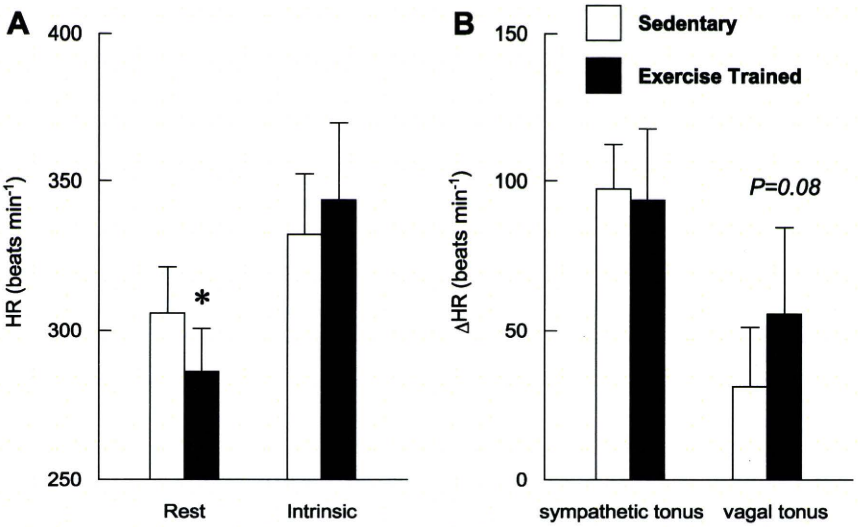

Fig. 1. Heart rate (HR) at rest and intrinsic HR (*A*) and HR sympathetic and vagal tone (*B*) obtained in sedentary and exercised-trained rats. *$P < 0.05$ compared with sedentary group.

DISCUSSION

We have examined the dynamic transfer function of autonomic HR control by using random binary sympathetic and vagal nerve stimulation in sedentary and exercised-trained rats. The major findings in the present study are *1*) that the exercise training did not alter the sympathetic transfer function substantially but augmented the dynamic gain of the vagal transfer function; and *2*) in the frequency domain, exercise training increased the dynamic HR response to vagal stimulation but not sympathetic stimulation, regardless of the frequency band. These findings are the first quantitative data on the effect of exercise training on the dynamic characteristics of peripheral HR control by the sympathetic and vagal systems.

Validity of Exercise Training

The relative ventricular hypertrophy and higher exercise capacity in the exercised-trained compared with the sedentary group suggested that exercise program used in the present study was sufficient to induce physiological adaptations commensurate with an effective training stimulus. As is well known, exercise training induces bradycardia at rest (Fig. 1*A*). Moreover, changes in the spectral parameters for R-R interval (Table 2) and autonomic tone (Fig. 1*B*) induced by the exercise training are consistent with earlier studies in rats (30, 31).

Effect of Exercise Training on Sympathetic and Vagal Transfer Function

Exercise training altered neither dynamic (Fig. 2) nor static sympathetic transfer function (Fig. 5*A*). These results are different than those reported in a previous study in which swim training significantly reduced the HR response to sympathetic nerve stimulation in a double atrial/right stellate ganglion preparation in guinea pigs (22). The discrepancy between investigations may have arisen from differences in the nerves experimentally stimulated (cervical sympathetic nerve vs. stellate ganglion), animal species studied (rats vs. guinea pigs), and/or experimental preparation utilized (in vivo vs. ex vivo). The mechanisms underlying the sympathetically mediated exercise training effect on HR are also controversial. For instance, chronotropic responsiveness to isoproterenol has been reported to be decreased in one study (15) but unchanged in another (22) by exercise training. Furthermore, in response to exercise training, the density and affinity of β-adrenoceptors in the heart have been shown to be reduced in some reports (26, 33), while unchanged in others (3, 34, 35).

Table 3. *Arterial pressure(AP) and heart rate (HR) during dynamic sympathetic stimulation protocol*

	Sedentary		Exercise Trained	
	Prestimulation	During Stimulation	Prestimulation	During Stimulation
AP, mmHg	74 ± 16	68 ± 15†	89 ± 17	84 ± 24
HR, beats/min	377 ± 25	444 ± 23†	381 ± 16	444 ± 26†

Values are means ± SD. †$P < 0.05$ compared with prestimulation.

Exercise training augmented the dynamic gain of the vagal transfer function (Fig. 2). The effect of exercise training was also significant for static vagal transfer function (Fig. 5*B*). These results are in agreement with previous studies showing that exercise training significantly augmented the HR response to vagal nerve stimulation in a double atrial/right vagal nerve preparation using mice (9, 10). In contrast, Negrao et al. (25) demonstrated that the HR response to vagal stimulation was depressed in exercised-trained rats. A possible explanation for this disparate result is that the arterial baroreflexes remained intact in the experimental preparation used in the study (25). In contrast, sinoaortic barodenervation was performed in the present investigation to minimize baroreflex-mediated changes in sympathetic efferent nerve activity. Exercise training has been shown to attenuate the baroreflex-mediated sympathetic nerve response to hypotension (11). Although speculative, in the study by Negrao et al. (25), baroreflex-mediated sympathetic activation in response to vagally-induced hypotension might have been less in exercised-trained compared with sedentary rats. Consequently, the gain of vagal stimulation might have been attenuated in exercised-trained animals relative to sedentary rats. This suggestion is reasonable given that accentuated antagonism is indicative of a diminution in background sym-

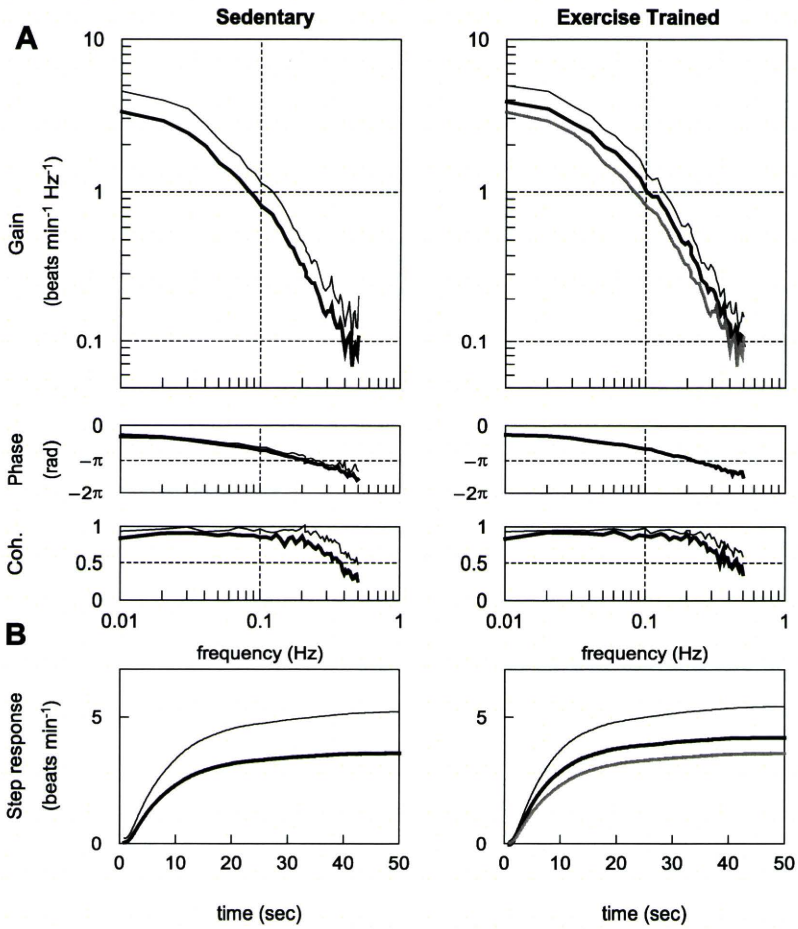

Fig. 2. *A*: transfer function from sympathetic stimulation to the HR response obtained in sedentary and exercised-trained rats. Gains (*top*), phase shifts (*middle*), and coherence (Coh.) functions (*bottom*) are presented. *B*: calculated step response to 1-Hz tonic sympathetic stimulation. Thick lines represent the mean, whereas thin lines indicate ± SD values. The gray solid curves in the gain and step response panels (*right*) duplicates the means (*left*).

pathetic tonus, which can decrease the gain of the vagal transfer function (17).

It has been documented that the intensity of exercise as well as the duration of exercise training are related to the autonomic adaptation to exercise training (28). These factors have been shown to be largely variable among different studies. A well-controlled experimental setup is needed to clarify these issues.

Dynamic Gain Values of Sympathetic and Vagal Transfer Functions Corresponding to HRV Frequency Bands

HRV is considered to reflect autonomic tone (19). The VLF component is likely to reflect changes in vasomotor tone in relation to thermoregulation and local adjustment of resistance in individual vascular beds; the LF component is considered to be a marker of sympathetic activity, although it remains a matter of debate; and the HF component mainly originates from respiratory activity and is considered to be mediated by vagal input (27). In rats, Cerutti et al. (8) determined that the LF component ranged between 0.27 and 0.74 Hz, and the HF component was > 0.75 Hz.

Averaged dynamic gain values of sympathetic transfer function for VLF and LF bands did not differ between the sedentary and exercised-trained groups (Fig. 4*A*). These results suggest that changes in the peripheral sympathetic control of HR likely do not contribute significantly to training-induced alterations in HRV. Therefore, the lower percentage of LF power and LF/HF ratio in the exercised-trained group (Table 2) may indicate reduced activation of sympathetic outflow from autonomic centers (23). In contrast, averaged dynamic gain values of vagal transfer function for VLF, LF, and HF bands (Fig. 4*B*) as

Table 4. *Sympathetic transfer function parameters and step response*

	Sedentary	Exercise Trained
Gain, beats·min^{-1}·Hz^{-1}	4.2 ± 1.5	4.5 ± 1.5
Natural frequency, Hz	0.07 ± 0.01	0.08 ± 0.01
Damping ratio	1.96 ± 0.55	1.69 ± 0.15
Lag time, s	0.71 ± 0.10	0.62 ± 0.11
Steady-state response, beats/min	3.6 ± 1.6	4.2 ± 1.2
80% rise time, s	12.9 ± 2.7	12.1 ± 3.0

Values are means ± SD. See APPENDIX for transfer function parameters.

Table 5. *AP and HR during dynamic vagal stimulation protocol*

	Sedentary		Exercise Trained	
	Prestimulation	During stimulation	Prestimulation	During stimulation
AP, mmHg	72 ± 21	68 ± 15	92 ± 14	80 ± 21
HR, beats/min	373 ± 18	327 ± 38 †	372 ± 14	301 ± 32 †

Values are means ± SD. †$P < 0.05$ compared with prestimulation.

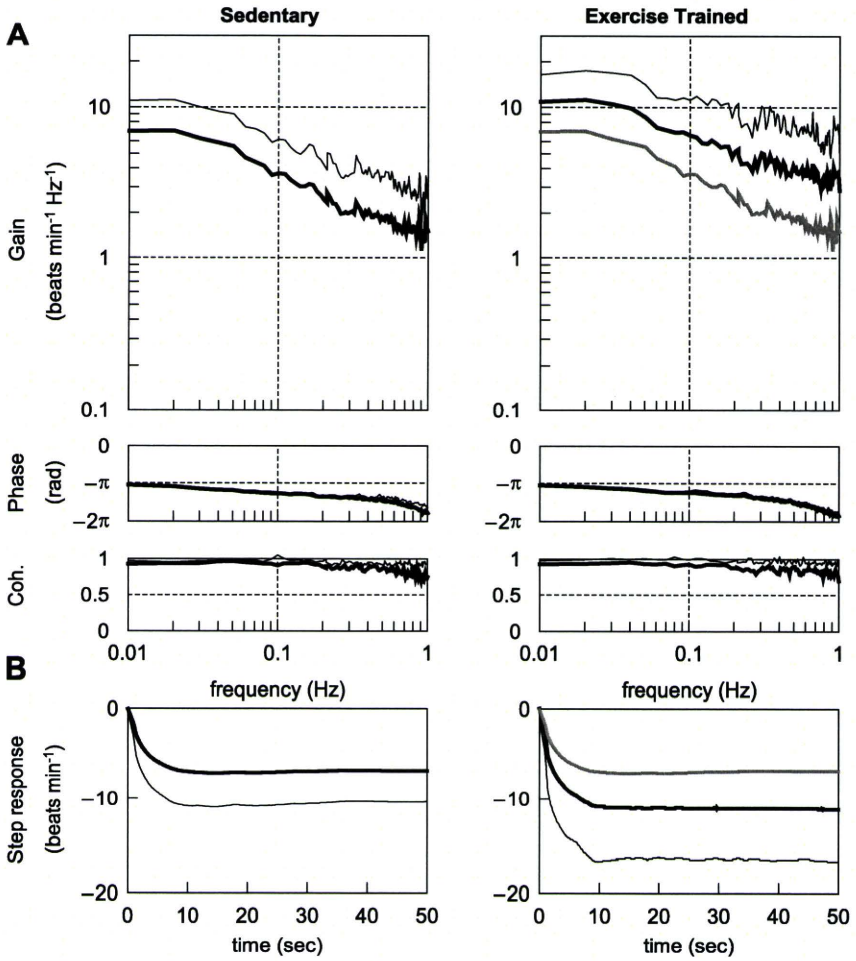

Fig. 3. *A*: transfer function from vagal stimulation to the HR response obtained in sedentary and exercised-trained rats. Gains (*top*), phase shifts (*middle*), and coherence functions (*bottom*) are presented. *B*: calculated step response to 1-Hz tonic vagal stimulation. Thick lines represent the mean, whereas thin lines indicate ± SD values. The gray solid curves in the gain and step response panels (*right*) duplicate the means (*left*).

well as the percentage of HF power (Table 2) were significantly greater in the exercised-trained compared with the sedentary group. These results suggest that the augmentation in HRV induced by exercise training is, at least in part, mediated by augmentations in the peripheral vagal control of HR.

What are the possible mechanisms underlying augmentations in the peripheral vagal control of HR? Danson and Paterson (10) have presented evidence that neuronal nitric oxide synthase may be a key enzymatic protein underlying such training-induced increases in cardiac vagal function. This group has also demonstrated that HR changes in response to vagal stimulation are enhanced by exercise training in wild-type mice but not in heterozygous neuronal nitric oxide synthase knockout mice (9). Another candidate for augmentations in the peripheral vagal control of HR is muscarinic receptors, which play a fundamental role in HR control via vagally mediated regulation. However, the effects of exercise training have been inconsistent among studies, showing both increases (12) and no change (2, 3) in muscarinic receptors in the myocardium of rats. The possibility cannot be dismissed that training-induced changes in the activity of afferent inputs mediating vagal outflow may also contribute to the alterations in HRV (4). Further investigation is needed to clarify these issues.

Table 6. *Vagal transfer function parameters and step response*

	Sedentary	Exercise Trained
Gain, beats·min^{-1}·Hz^{-1}	6.1 ± 3.0	9.7 ± 5.1#
Corner frequency, Hz	0.11 ± 0.05	0.17 ± 0.09
Lag time, s	0.10 ± 0.08	0.17 ± 0.08
Steady-state response, beats/min	−6.7 ± 3.6	−11.2 ± 5.7#
80% Fall time, s	4.3 ± 2.2	4.3 ± 1.5

Values are means ± SD. #P = 0.06 compared with sedentary group. See APPENDIX for transfer function parameters.

Perspectives and Significance

To date, the mechanisms underlying increased HRV after exercise training remain to be elucidated. HRV may reflect both the autonomic outflow from the central nervous system and the peripheral autonomic regulation of atrial pacemaker cells. In human studies, it is difficult to separately examine each factor. The findings of the present study suggest that the augmentation in HRV induced by exercise training is, at least in part, mediated by augmentations in the peripheral vagal control of HR. In other words, even if vagal outflow from the central nervous system remains unchanged after exercise training, HRV could be increased by an enhanced responsiveness in the peripheral vagal, but not sympathetic, regulation of HR.

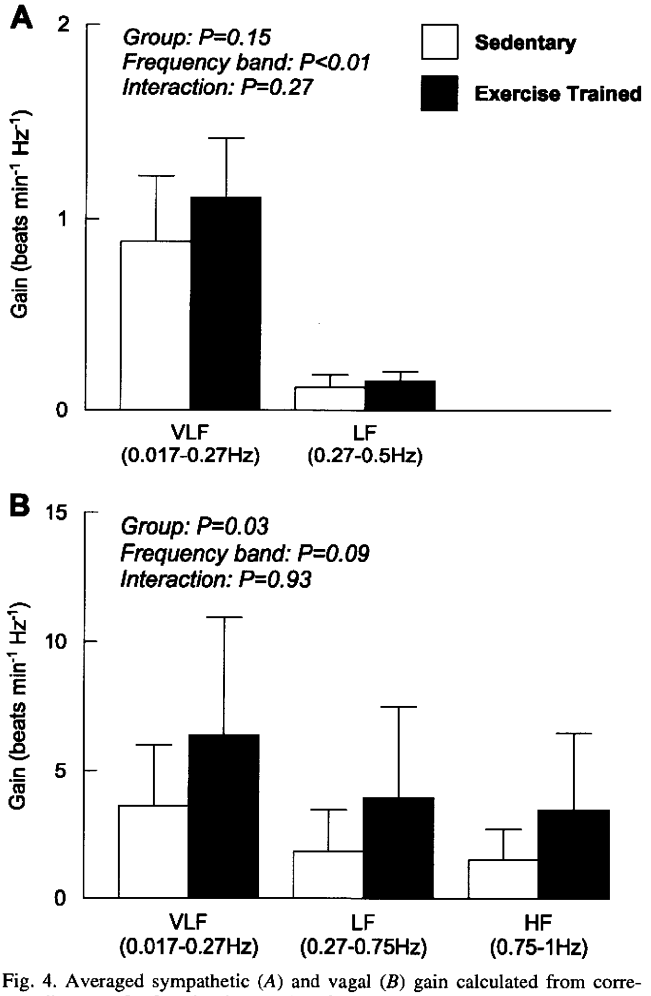

Fig. 4. Averaged sympathetic (*A*) and vagal (*B*) gain calculated from corresponding transfer function in very low frequency (VLF), low frequency (LF), and high frequency (HF) bands.

It has been well documented that decreased HRV is observed in heart failure (18) as well as in a variety of lifestyle-related diseases such as diabetes (16), hypertension (24), and obesity (1). Furthermore, reductions in HRV are related to increases in mortality rates as well as the occurrence of adverse cardiac events (32). Exercise training-induced augmentations in HRV maintain the potential to partially correct or normalize the autonomic dysfunction manifest in these disease states (4). Understanding the mechanisms contributing to the alterations in HRV induced by exercise training may significantly impact the development of novel therapeutic strategies for the treatment of autonomic dysfunction.

Limitations

There are several limitations to this study. First, the rats were slightly hyperventilated throughout the stimulation protocol. We cannot rule out the possibility that the hyperventilation might have affected the results reported. Second, dynamic sympathetic stimulation lowered mean AP in sedentary rats although sinoaortic barodenervation was performed. This may be explained by a possible difference in left ventricular functional capacity. For example, under conditions of equivalent HR, changes in systolic blood pressure were smaller in sedentary rats compared with exercised-trained rats (13). Third, the stimulation amplitude was fixed at 10 V for both sympathetic and vagal nerve stimulation. It should be noted, however, that our preliminary results indicated that 10 V was sufficiently large enough to evoke maximal HR responses. Fourth, transfer function data were obtained from anesthetized animals. This must be taken into account when interpreting the present results as anesthesia may affect the peripheral autonomic regulation of atrial pacemaker cells. Finally, we stimulated the sympathetic and vagal nerves according to a binary white noise signal. Although this method of stimulation is quite different from the physiological pattern of neuronal discharge, the coherence was near unity over the frequency range of interest. This finding indicates that the system properties do not vary considerably in response to different patterns of stimulation.

Conclusion

In the present study, it was demonstrated for the first time that exercise training did not alter dynamic sympathetic control of HR, while it did augment dynamic vagal control of HR. In addition, the group effect was significant with regard to the dynamic gain values for the vagal transfer functions corresponding to VLF, LF, and HF bands. This finding suggests that enhancements in the peripheral vagal control of HR may, at

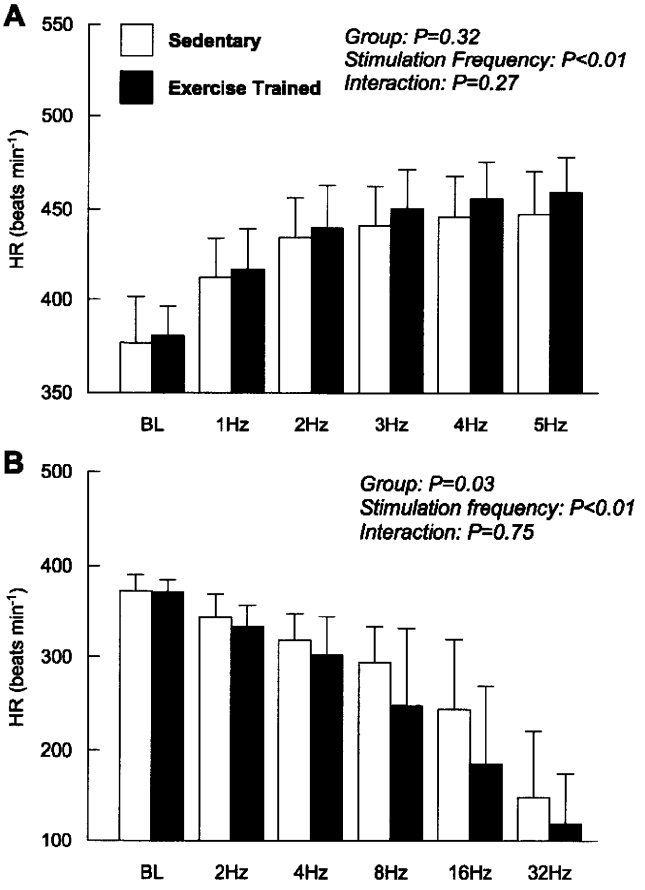

Fig. 5. HR response to stepwise sympathetic (*A*) and vagal (*B*) stimulation obtained in sedentary and exercised-trained rats.

least in part, contribute to the exercise-induced augmentation in HRV in healthy rats.

APPENDIX: TRANSFER FUNCTION ANALYSIS

The dynamic transfer function from binary white noise stimulation to the HR response was estimated based on the following procedure. Input-output data pairs of the stimulation frequency and HR were resampled at 10 Hz to be consistent with our previous study (21). Subsequently, data pairs were partitioned into eight 50% overlapping segments consisting of 1,024 data points each. For each segment, the linear trend was subtracted and a Hanning window was applied. A fast Fourier transform was then performed to obtain the frequency spectra of nerve stimulation [$N(f)$] and HR [$HR(f)$]. Over the eight segments, the power of the nerve stimulation [$S_{N\cdot N}(f)$], the power of the HR [$S_{HR\cdot HR}(f)$], and the cross-power between these two signals [$S_{N\cdot HR}(f)$] were ensemble averaged. Finally, the transfer function [$H(f)$] from nerve stimulation to the HR response was determined using the following equation (20).

$$H(f) = \frac{S_{N\text{-}HR}(f)}{S_{N\text{-}N}(f)}$$

To quantify the linear dependence of the HR response on vagal or sympathetic stimulation, the magnitude-squared coherence function [Coh(f)] was estimated employing the following equation (20).

$$\mathrm{Coh}(f) = \frac{|S_{\mathrm{N\text{-}HR}}(f)|^2}{S_{\mathrm{N\cdot N}}(f) \cdot S_{\mathrm{HR\cdot HR}}(f)}$$

Coherence values range from zero to unity. Unity coherence indicates perfect linear dependence between the input and output signals; in contrast, zero coherence indicates total independence between the two signals.

Since the transfer function from sympathetic stimulation to HR response in rats approximated a second order low-pass filter with pure delay (21), we determined the parameters of the sympathetic transfer function using the following equation.

$$H(f) = \frac{K}{1 + 2\zeta\frac{f}{f_N}\mathrm{j} + \left(\frac{f}{f_N}\mathrm{j}\right)^2} e^{-2\pi f\mathrm{j}L}$$

where K is dynamic gain (in beats·min^{-1}·Hz^{-1}), f_N is the natural frequency (in Hz), ζ is the damping ratio, L is lag time (in s), and f and j represent frequency and imaginary units, respectively. These parameters were estimated by means of an iterative nonlinear least squares regression.

Since the transfer function from vagal stimulation to HR response in rats approximated a first-order, low-pass filter with pure delay (21), we determined the parameters of the vagal transfer function using the following equation.

$$H(f) = \frac{-K}{1 + \frac{f}{f_C}\mathrm{j}} e^{-2\pi f\mathrm{j}L}$$

where K represents the dynamic gain (in beats·min^{-1}·Hz^{-1}), fc denotes the corner frequency (in Hz), L denotes the lag time (in s), and f and j represent frequency and imaginary units, respectively. The negative sign in the numerator indicates the negative HR response to vagal stimulation. These parameters were estimated by means of an iterative nonlinear least squares regression.

GRANTS

This study was supported by Health and Labor Sciences Research Grants H18-nano-Ippan-003, H19-nano-Ippan-009, H20-katsudo-Shitei-007, and H21-nano-Ippan-005 from the Ministry of Health, Labor and Welfare of Japan, by Grants-in-Aid for Scientific Research No. 19700559 from the Ministry of Education, Culture, Sports, Science and Technology in Japan, and by the Industrial Technology Research Grant Program from New Energy and Industrial Technology Development Organization of Japan. M. Mizuno was supported from Research Fellowships of the Japan Society for the Promotion of Science for Young Scientists.

DISCLOSURES

No conflicts of interest, financial or otherwise, are declared by the author(s).

REFERENCES

1. **Arone LJ, Mackintosh R, Rosenbaum M, Leibel RL, Hirsch J.** Autonomic nervous system activity in weight gain and weight loss. *Am J Physiol Regul Integr Comp Physiol* 269: R222–R225, 1995.
2. **Barbier J, Rannou-Bekono F, Marchais J, Berthon PM, Delamarche P, Carre F.** Effect of training on β1-, β2-, β3-adrenergic and M2 muscarinic receptors in rat heart. *Med Sci Sports Exerc* 36: 949–954, 2004.
3. **Barbier J, Reland S, Ville N, Rannou-Bekono F, Wong S, Carre F.** The effects of exercise training on myocardial adrenergic and muscarinic receptors. *Clin Auton Res* 16: 61–65, 2006.
4. **Billman GE.** Cardiac autonomic neural remodeling and susceptibility to sudden cardiac death: effect of endurance exercise training. *Am J Physiol Heart Circ Physiol* 297: H1171–H1193, 2009.
5. **Blomqvist CG, Saltin B.** Cardiovascular adaptations to physical training. *Annu Rev Physiol* 45: 169–189, 1983.
6. **Brenner DA, Apstein CS, Saupe KW.** Exercise training attenuates age-associated diastolic dysfunction in rats. *Circulation* 104: 221–226, 2001.
7. **Buch AN, Coote JH, Townend JN.** Mortality, cardiac vagal control and physical training–what's the link? *Exp Physiol* 87: 423–435, 2002.
8. **Cerutti C, Gustin MP, Paultre CZ, Lo M, Julien C, Vincent M, Sassard J.** Autonomic nervous system and cardiovascular variability in rats: a spectral analysis approach. *Am J Physiol Heart Circ Physiol* 261: H1292–H1299, 1991.
9. **Danson EJ, Mankia KS, Golding S, Dawson T, Everatt L, Cai S, Channon KM, Paterson DJ.** Impaired regulation of neuronal nitric oxide synthase and heart rate during exercise in mice lacking one nNOS allele. *J Physiol* 558: 963–974, 2004.
10. **Danson EJ, Paterson DJ.** Enhanced neuronal nitric oxide synthase expression is central to cardiac vagal phenotype in exercise-trained mice. *J Physiol* 546: 225–232, 2003.
11. **DiCarlo SE, Bishop VS.** Exercise training attenuates baroreflex regulation of nerve activity in rabbits. *Am J Physiol Heart Circ Physiol* 255: H974–H979, 1988.
12. **Favret F, Henderson KK, Clancy RL, Richalet JP, Gonzalez NC.** Exercise training alters the effect of chronic hypoxia on myocardial adrenergic and muscarinic receptor number. *J Appl Physiol* 91: 1283–1288, 2001.
13. **Fitzsimons DP, Bodell PW, Herrick RE, Baldwin KM.** Left ventricular functional capacity in the endurance-trained rodent. *J Appl Physiol* 69: 305–312, 1990.
14. **Goldsmith RL, Bigger JT Jr, Steinman RC, Fleiss JL.** Comparison of 24-hour parasympathetic activity in endurance-trained and untrained young men. *J Am Coll Cardiol* 20: 552–558, 1992.
15. **Hammond HK, White FC, Brunton LL, Longhurst JC.** Association of decreased myocardial β-receptors and chronotropic response to isoproterenol and exercise in pigs following chronic dynamic exercise. *Circ Res* 60: 720–726, 1987.
16. **Ikeda T, Matsubara T, Sato Y, Sakamoto N.** Circadian blood pressure variation in diabetic patients with autonomic neuropathy. *J Hypertens* 11: 581–587, 1993.
17. **Kawada T, Ikeda Y, Sugimachi M, Shishido T, Kawaguchi O, Yamazaki T, Alexander J Jr, Sunagawa K.** Bidirectional augmentation of heart rate regulation by autonomic nervous system in rabbits. *Am J Physiol Heart Circ Physiol* 271: H288–H295, 1996.
18. **La Rovere MT, Pinna GD, Maestri R, Mortara A, Capomolla S, Febo O, Ferrari R, Franchini M, Gnemmi M, Opasich C, Riccardi PG, Traversi E, Cobelli F.** Short-term heart rate variability strongly predicts sudden cardiac death in chronic heart failure patients. *Circulation* 107: 565–570, 2003.

19. **Malliani A, Pagani M, Lombardi F, Cerutti S.** Cardiovascular neural regulation explored in the frequency domain. *Circulation* 84: 482–492, 1991.
20. **Marmarelis P, Marmarelis V.** The white noise method in system identification. In: *Analysis of Physiological Systems*. New York: Plenum, 1978, p. 131–221.
21. **Mizuno M, Kawada T, Kamiya A, Miyamoto T, Shimizu S, Shishido T, Smith SA, Sugimachi M.** Dynamic characteristics of heart rate control by the autonomic nervous system in rats. *Exp Physiol* 95: 919–925, 2010.
22. **Mohan RM, Choate JK, Golding S, Herring N, Casadei B, Paterson DJ.** Peripheral pre-synaptic pathway reduces the heart rate response to sympathetic activation following exercise training: role of NO. *Cardiovasc Res* 47: 90–98, 2000.
23. **Mueller PJ.** Exercise training attenuates increases in lumbar sympathetic nerve activity produced by stimulation of the rostral ventrolateral medulla. *J Appl Physiol* 102: 803–813, 2007.
24. **Mussalo H, Vanninen E, Ikaheimo R, Laitinen T, Laakso M, Lansimies E, Hartikainen J.** Heart rate variability and its determinants in patients with severe or mild essential hypertension. *Clin Physiol* 21: 594–604, 2001.
25. **Negrao CE, Moreira ED, Santos MC, Farah VM, Krieger EM.** Vagal function impairment after exercise training. *J Appl Physiol* 72: 1749–1753, 1992.
26. **Nieto JL, Laviada ID, Guillen A, Haro A.** Adenylyl cyclase system is affected differently by endurance physical training in heart and adipose tissue. *Biochem Pharmacol* 51: 1321–1329, 1996.
27. **Pagani M, Lombardi F, Guzzetti S, Rimoldi O, Furlan R, Pizzinelli P, Sandrone G, Malfatto G, Dell'Orto S, Piccaluga E.** Power spectral analysis of heart rate and arterial pressure variabilities as a marker of sympatho-vagal interaction in man and conscious dog. *Circ Res* 59: 178–193, 1986.
28. **Sandercock GR, Bromley PD, Brodie DA.** Effects of exercise on heart rate variability: inferences from meta-analysis. *Med Sci Sports Exerc* 37: 433–439, 2005.
29. **Schwarz P, Diem R, Dun NJ, Forstermann U.** Endogenous and exogenous nitric oxide inhibits norepinephrine release from rat heart sympathetic nerves. *Circ Res* 77: 841–848, 1995.
30. **Souza SB, Flues K, Paulini J, Mostarda C, Rodrigues B, Souza LE, Irigoyen MC, De Angelis K.** Role of exercise training in cardiovascular autonomic dysfunction and mortality in diabetic ovariectomized rats. *Hypertension* 50: 786–791, 2007.
31. **Tezini GC, Silveira LC, Villa-Cle PG Jr, Jacinto CP, Di Sacco TH, Souza HC.** The effect of aerobic physical training on cardiac autonomic control of rats submitted to ovariectomy. *Menopause* 16: 110–116, 2009.
32. **Tsuji H, Larson MG, Venditti FJ Jr, Manders ES, Evans JC, Feldman CL, Levy D.** Impact of reduced heart rate variability on risk for cardiac events. The Framingham Heart Study. *Circulation* 94: 2850–2855, 1996.
33. **Werle EO, Strobel G, Weicker H.** Decrease in rat cardiac β1- and β2-adrenoceptors by training and endurance exercise. *Life Sci* 46: 9–17, 1990.
34. **Williams RS.** Physical conditioning and membrane receptors for cardioregulatory hormones. *Cardiovasc Res* 14: 177–182, 1980.
35. **Williams RS, Schaible TF, Bishop T, Morey M.** Effects of endurance training on cholinergic and adrenergic receptors of rat heart. *J Mol Cell Cardiol* 16: 395–403, 1984.
36. **Yamamoto K, Miyachi M, Saitoh T, Yoshioka A, Onodera S.** Effects of endurance training on resting and post-exercise cardiac autonomic control. *Med Sci Sports Exerc* 33: 1496–1502, 2001.

Japan J. Indust. Appl. Math. (2011) 28:89–117
DOI 10.1007/s13160-011-0024-2

ORIGINAL PAPER

Area 3

Convergence analysis of inexact LU-type preconditioners for indefinite problems arising in incompressible continuum analysis

Takumi Washio · Toshiaki Hisada

Received: 26 June 2009 / Revised: 6 October 2009 / Published online: 25 February 2011

Abstract Developing efficient solution methods for indefinite problems arising in constraint problems is an important issue in incompressible or nearly incompressible continuum analysis. In this paper, we first compare the convergence properties of two classical iterative approaches, namely the inexact block triangular algorithm and the inexact block LU algorithm. It is shown that the latter can be applied under more relaxed conditions than the former. We further analyze properties of the latter algorithm when applied as a preconditioner for Krylov subspace methods. Similar to the analysis of the inexact block LU preconditioner, we also analyze the properties of a fill-controlled incomplete LU preconditioner. The theoretical convergence estimates are validated and the performance of the two LU-type preconditioners are compared through numerical experiments with large deformation problems of a hyper-elastic material.

Keywords Saddle point problem · Block LU factorization · Incompressible hyper-elastic material

Mathematics Subject Classification (2000) 65F08 · 65N12

T. Washio (✉)
Graduate School of Frontier Science, University of Tokyo,
5-1-5 Kashiwanoha, Kashiwa, Chiba 277-0882, Japan
e-mail: washio@sml.k.u-tokyo.ac.jp

T. Hisada
Graduate School of Frontier Science, University of Tokyo,
7-3-1 Hongo, Bunkyo-ku, Tokyo 113-0033, Japan

1 Introduction

In this paper, we deal with a saddle point linear system in a finite dimensional space:

$$\begin{bmatrix} \mathbf{A} & \mathbf{B}^T \\ \mathbf{B} & \mathbf{0} \end{bmatrix} \begin{bmatrix} X \\ Y \end{bmatrix} = \begin{bmatrix} F \\ G \end{bmatrix}. \tag{1}$$

Furthermore, we assume that $\mathbf{A}$ is an $m \times m$ symmetric positive definite matrix, and $\mathbf{B}$ is an $n \times m$ full rank matrix, where $m > n$. By applying complete block LU factorization to this 2×2 block matrix, we have

$$\mathcal{A} = \begin{bmatrix} \mathbf{A} & \mathbf{B}^T \\ \mathbf{B} & \mathbf{0} \end{bmatrix} = \begin{bmatrix} \mathbf{I} & \mathbf{0} \\ \mathbf{B}\mathbf{A}^{-1} & \mathbf{I} \end{bmatrix} \begin{bmatrix} \mathbf{A} & \mathbf{0} \\ \mathbf{0} & -\mathbf{S} \end{bmatrix} \begin{bmatrix} \mathbf{I} & \mathbf{A}^{-1}\mathbf{B}^T \\ \mathbf{0} & \mathbf{I} \end{bmatrix}, \tag{2}$$

where $\mathbf{S}$ is the Schur complement defined as

$$\mathbf{S} = \mathbf{B}\mathbf{A}^{-1}\mathbf{B}^T. \tag{3}$$

From Sylvester's law of inertia, we see that the numbers of positive and negative eigenvalues of the coefficient matrix in Eq. (1) are m and n, respectively. Thus, the matrix is indefinite.

This type of problem arises in analysis of incompressible continuum like industrial hyper-elastic materials, living tissues, fluids, etc. In this problem, though the first diagonal block $\mathbf{A}$ is positive, the total matrix is indefinite. Thus, special cares are required in construction and convergence analysis of iterative methods since the iterative solution strategy based on energy minimization as applied to the conjugate gradient method is not valid. The target of this paper is to analyze convergence properties of some efficient iterative solution methods for these problems and to validate the convergence estimation results through numerical experiments. In general, Eq. (1) is a typical linear system that appears in the solution process of a minimization problem with constraints and is reviewed briefly below. In the above mentioned cases of the incompressible materials, the constraints correspond to the incompressibility. Let us assume that we wish to find the minimum of a given functional $E(\mathbf{u})$ under constraints represented by $\mathbf{C}(\mathbf{u}) = \mathbf{0}$, where $\mathbf{u}$ is in m-dimensional space and $\mathbf{C}$ is an n-dimensional vector function. From the Lagrange multiplier method, we see that the solution $\mathbf{u}$ is given as a stationary point of the Lagrange functional:

$$L(\mathbf{u}, \lambda) = E(\mathbf{u}) + \mathbf{C}(\mathbf{u})^T \lambda, \tag{4}$$

where λ is an n-dimensional vector called the Lagrange multiplier. Thus, by taking derivatives by $\mathbf{u}$ and λ, respectively, we obtain a system of nonlinear equations:

$$\frac{\partial E}{\partial \mathbf{u}}(\mathbf{u}) + \frac{\partial \mathbf{C}}{\partial \mathbf{u}}(\mathbf{u})^T \lambda = \mathbf{0}, \tag{5}$$

$$\mathbf{C}(\mathbf{u}) = \mathbf{0}. \tag{6}$$

This nonlinear problem can be solved iteratively by the Newton–Raphson method. Let $\mathbf{u}_k$ and λ_k be approximate solution vectors at the kth iteration. Then, by linearizing

the functions in Eqs. (5) and (6), the updates $X = \mathbf{u}_{k+1} - \mathbf{u}_k$ and $Y = \lambda_{k+1} - \lambda_k$ are obtained by solving the linear system in Eq. (1) with

$$\mathbf{A} = \frac{\partial^2 E}{\partial \mathbf{u}^2}(\mathbf{u}_k) + \frac{\partial^2 \mathbf{C}}{\partial \mathbf{u}^2}(u_k)^T \lambda_k, \tag{7}$$

$$\mathbf{B} = \frac{\partial \mathbf{C}}{\partial \mathbf{u}}(\mathbf{u}_k), \tag{8}$$

$$F = -\left(\frac{\partial E}{\partial \mathbf{u}}(\mathbf{u}_k) + \frac{\partial \mathbf{C}}{\partial \mathbf{u}}(\mathbf{u}_k)^T \lambda_k\right), \tag{9}$$

$$G = -\mathbf{C}(\mathbf{u}_k). \tag{10}$$

The solution process given above is typical of the procedure used in dealing with large deformation problems of incompressible hyper-elastic materials using a finite element method, in which the Lagrange multiplier is hydrostatic pressure. Also, in incompressible fluid analysis, although $\mathbf{A}$ is not generally symmetric due to the presence of a convection term in the Navier–Stokes equation and thus it cannot be formulated as an optimization problem, Eq. (1) still arises due to the incompressibility, with the second block variable being fluid pressure.

An inherent difficulty in constructing an iterative block-by-block relaxation for Eq. (1) arises from the zero diagonal block in the second row. With regards a solution candidate for the first block, there is no way of computing the solution for the second block from the equation on the second row only. However, the factorization of $\mathcal{A}$ in Eq. (2) provides a hint for constructing an approximate matrix $\mathcal{P}$ to the coefficient matrix $\mathcal{A}$ as follows.

$$\mathcal{P} = \begin{cases} \mathcal{P}_{\mathrm{T}} = \begin{bmatrix} \mathbf{I} & \mathbf{0} \\ \mathbf{B}\mathbf{Q}_A^{-1} & \mathbf{I} \end{bmatrix} \begin{bmatrix} \mathbf{Q}_A & \mathbf{0} \\ \mathbf{0} & -\mathbf{Q}_B \end{bmatrix} \\ \mathcal{P}_{\mathrm{S}} = \begin{bmatrix} \mathbf{I} & \mathbf{0} \\ \mathbf{B}\mathbf{Q}_A^{-1} & \mathbf{I} \end{bmatrix} \begin{bmatrix} \mathbf{Q}_A & \mathbf{0} \\ \mathbf{0} & -\mathbf{Q}_B \end{bmatrix} \begin{bmatrix} \mathbf{I} & \mathbf{Q}_A^{-1}\mathbf{B}^T \\ \mathbf{0} & \mathbf{I} \end{bmatrix}. \end{cases} \tag{11}$$

Here, $\mathbf{Q}_A$ and $\mathbf{Q}_B$ are approximations of $\mathbf{A}$ and $\mathbf{S}$, respectively. The approximation $\mathcal{P}_{\mathrm{S}}$ is obtained by replacing $\mathbf{A}$ and $\mathbf{S}$ in Eq. (2) with $\mathbf{Q}_A$ and $\mathbf{Q}_B$, respectively, while $\mathcal{P}_{\mathrm{T}}$ is found by taking the lower block triangular part thereof. The iterative process based on the matrix splitting:

$$\mathcal{P}\begin{bmatrix} X_{i+1} \\ Y_{i+1} \end{bmatrix} + (\mathcal{A} - \mathcal{P})\begin{bmatrix} X_i \\ Y_i \end{bmatrix} = \begin{bmatrix} F \\ G \end{bmatrix} \tag{12}$$

is written as

$$\begin{cases} X_{i+1} = X_i + \mathbf{Q}_A^{-1}(F - (\mathbf{A}X_i + \mathbf{B}^T Y_i)), \\ Y_{i+1} = Y_i + \mathbf{Q}_B^{-1}(\mathbf{B}X_{i+1} - G) \end{cases} \tag{13}$$

for $\mathcal{P}_{\mathrm{T}}$, and

$$\begin{cases} X_{i+1/2} = X_i + \mathbf{Q}_A^{-1}(F - (\mathbf{A}X_i + \mathbf{B}^T Y_i)), \\ Y_{i+1} \quad = Y_i + \mathbf{Q}_B^{-1}(\mathbf{B}X_{i+1/2} - G), \\ X_{i+1} \quad = X_{i+1/2} - \mathbf{Q}_A^{-1}\mathbf{B}^T(Y_{i+1} - Y_i) \end{cases} \tag{14}$$

for $\mathcal{P}_{\mathrm{S}}$. The former iterative process, known as the inexact Uzawa algorithm, was proposed and its convergence property analyzed by Bramble et al. [3]. The latter process has, for example, been applied as a preconditioner for the Krylov subspace method to CFD applications by Little et al. [9], and to fluid structure interaction problems by Washio et al. [14]. Hereafter, we refer to the former and latter algorithms as the inexact block triangular and inexact block LU algorithms, respectively. The first purpose of this paper is to analyze the convergence property of Eq. (14) by applying similar approaches to those given in [3]. We identify substantial differences in the required conditions on $\mathbf{Q}_A$ and $\mathbf{Q}_B$ to ensure the convergence of the iterative processes between the two approaches. It is also shown that error reduction analysis can be performed under more reasonable norms for $\mathcal{P}_{\mathrm{S}}$ than for $\mathcal{P}_{\mathrm{T}}$. Furthermore, the convergence condition for Eq. (13) is slightly more relaxed than the one given in [3].

In addition to the convergence analysis, we analyze the eigenvalue distribution of the preconditioned matrix $\mathcal{P}_{\mathrm{S}}^{-1}\mathcal{A}$. This analysis provides a good indication of the convergence performance when $\mathcal{P}_{\mathrm{S}}$ is applied as a preconditioner for the Krylov subspace method. Although it is difficult to give an exact estimation of the convergence rate from the eigenvalue distribution alone, we identify the following interesting relations.

1. How the eigenvalue distribution is related to the degree of approximation of $\mathbf{Q}_A$ to $\mathbf{A}$ and $\mathbf{Q}_B$ to $\mathbf{B}\mathbf{Q}_A^{-1}\mathbf{B}^T$.
2. How various components of the eigenvalue distribution (for example, the minimal real part, maximal imaginary part, etc.) affect the convergence rate.

Many studies have focused on the convergence of the block-type (block diagonal, block triangle) preconditioners. Klawonn and Starke [8] estimated the convergence of GMRES with a block triangular preconditioner using field-of-values analysis. Elman et al. [5] studied the performance of a block triangular preconditioner through eigenvalue distribution analysis of the preconditioned system. Various studies by other researchers are surveyed in [2]. Most of these studies focus on fluid or linear elasticity problems, for which it is relatively easy to apply the cheaply invertible and well-approximated $\mathbf{Q}_A$ or $\mathbf{Q}_B$ by exploiting specific knowledge of the background PDEs or regularity of the computational grid. Here, 'well-approximated' implies spectral equivalence between $\mathbf{Q}_A$ and $\mathbf{A}$ or between $\mathbf{Q}_B$ and $\mathbf{S}$. In other words, the eigenvalues of $\mathbf{Q}_A^{-1}\mathbf{A}$ or $\mathbf{Q}_B^{-1}\mathbf{S}$ are contained in a positive interval whose end points do not depend on the mesh size. Such a cheaply invertible operator $\mathbf{Q}_A$ can easily be implemented, for example, by a multigrid cycle [6] if the grid is regular or if $\mathbf{A}$ is strongly diagonal dominant due to the presence of the inertia term in time-dependent problems [10].

In real-life nonlinear finite element continuum mechanics, the matrices $\mathbf{A}$ and $\mathbf{B}$ are produced through complicated computations of derivatives in Eqs. (7) and (8) on an unstructured grid. As a result, it is not easy to see the properties of the operators $\mathbf{A}$ and $\mathbf{B}$ which provide hints for constructing efficient $\mathbf{Q}_A$ and $\mathbf{Q}_B$ matrices. This makes

it difficult to define the cheaply invertible and well-approximated $\mathbf{Q}_A$ and $\mathbf{Q}_B$. Under such circumstances, it is important to estimate the convergence rate for the entire system, where the degree of approximation for either one or both of these matrices is poor.

In addition to the analysis of a block-type LU preconditioner, we also analyze a more easily implementable preconditioner that is defined by the standard element-wise incomplete LU (ILU) factorization under a specific fill-in strategy [14]. In this analysis, although we cannot give concrete estimations of the eigenvalue distribution, we do identify a clear difference from the block-type preconditioner. Through numerical experiments, we examine how this difference affects the convergence behavior.

2 Matrix splitting methods based on inexact block triangular and block LU matrices

Let $E_i^X = X - X_i$, $E_i^Y = Y - Y_i$ be errors for the iterative solutions in Eq. (12). Then, the iteration errors satisfy the following recurrence:

$$\begin{bmatrix} E_{i+1}^X \\ E_{i+1}^Y \end{bmatrix} = \mathcal{R} \begin{bmatrix} E_i^X \\ E_i^Y \end{bmatrix} \quad \text{with } \mathcal{R} = \mathcal{P}^{-1}(\mathcal{P} - \mathcal{A}). \tag{15}$$

The error reduction matrix $\mathcal{R}$ can be represented as

$$\mathcal{R}_{\mathrm{T}} = \begin{bmatrix} \mathbf{Q}_A^{-1} & \mathbf{0} \\ \mathbf{0} & -\mathbf{Q}_B^{-1} \end{bmatrix} \begin{bmatrix} \mathbf{I} & \mathbf{0} \\ -\mathbf{B}\mathbf{Q}_A^{-1} & \mathbf{I} \end{bmatrix} \begin{bmatrix} \mathbf{Q}_A - \mathbf{A} & -\mathbf{B}^T \\ \mathbf{0} & -\mathbf{Q}_B \end{bmatrix}$$

for $\mathcal{P}_{\mathrm{T}}$, and

$$\mathcal{R}_{\mathrm{S}} = \begin{bmatrix} \mathbf{I} & -\mathbf{Q}_A^{-1}\mathbf{B}^T \\ \mathbf{0} & \mathbf{I} \end{bmatrix} \begin{bmatrix} \mathbf{Q}_A^{-1} & \mathbf{0} \\ \mathbf{0} & -\mathbf{Q}_B^{-1} \end{bmatrix} \begin{bmatrix} \mathbf{I} & \mathbf{0} \\ -\mathbf{B}\mathbf{Q}_A^{-1} & \mathbf{I} \end{bmatrix} \begin{bmatrix} \mathbf{Q}_A - \mathbf{A} & \mathbf{0} \\ \mathbf{0} & \mathbf{B}\mathbf{Q}_A^{-1}\mathbf{B}^T - \mathbf{Q}_B \end{bmatrix}$$

for $\mathcal{P}_{\mathrm{S}}$. To simplify these expressions of the error reduction matrices, we introduce scaled matrices for $\mathbf{A}$ and $\mathbf{B}$ as follows.

$$\mathbf{M} = \mathbf{Q}_A^{-1/2}\mathbf{A}\mathbf{Q}_A^{-1/2}, \tag{16}$$

$$\mathbf{N} = \mathbf{Q}_B^{-1/2}\mathbf{B}\mathbf{Q}_A^{-1/2}. \tag{17}$$

Note that the following equality holds.

$$\mathbf{N}\mathbf{M}^{-1}\mathbf{N}^T = \mathbf{Q}_B^{-1/2}\mathbf{B}\mathbf{A}^{-1}\mathbf{B}^T\mathbf{Q}_B^{-1/2}.$$

Throughout this section, we assume that $\mathbf{A}$ and $\mathbf{B}\mathbf{A}^{-1}\mathbf{B}^T$ are correctly approximated by $\mathbf{Q}_A$ and $\mathbf{Q}_B$, respectively, as they lead the convergence when applied within the

individual subspaces. That is, we assume that the following conditions are satisfied.

$$0 < \underline{m}\mathbf{I} \leq \mathbf{M} \leq \overline{m}\mathbf{I},\ 0 < \exists\underline{m} \leq \exists\overline{m} < 2, \tag{18}$$

$$0 < \underline{n_m}\mathbf{I} \leq \mathbf{N}\mathbf{M}^{-1}\mathbf{N}^T \leq \overline{n_m}\mathbf{I},\ 0 < \exists\underline{n_m} \leq \exists\overline{n_m} < 2. \tag{19}$$

Note that throughout this paper, we apply the inequality sign to two symmetric matrices $\mathbf{S}_1$ and $\mathbf{S}_2$ such that

$$\mathbf{S}_1 \leq \mathbf{S}_2,$$

if

$$(V, \mathbf{S}_1 V) \leq (V, \mathbf{S}_2 V), \forall V$$

holds.

We start by finding appropriate similarity transformations for the error reduction matrices to facilitate the convergence analysis. First, we see that transformation with a simple block diagonal matrix gives

$$\begin{bmatrix} \mathbf{Q}_A^{1/2} & \mathbf{0} \\ \mathbf{0} & \mathbf{Q}_B^{1/2} \end{bmatrix} \mathcal{R}_{\mathrm{T}} \begin{bmatrix} \mathbf{Q}_A^{-1/2} & \mathbf{0} \\ \mathbf{0} & \mathbf{Q}_B^{-1/2} \end{bmatrix} = \begin{bmatrix} \mathbf{I} & \mathbf{0} \\ \mathbf{0} & -\mathbf{I} \end{bmatrix} \begin{bmatrix} \mathbf{I}-\mathbf{M} & -\mathbf{N}^T \\ -\mathbf{N}(\mathbf{I}-\mathbf{M}) & \mathbf{N}\mathbf{N}^T - \mathbf{I} \end{bmatrix} \tag{20}$$

and

$$\begin{aligned} &\begin{bmatrix} \mathbf{Q}_A^{1/2} & \mathbf{0} \\ \mathbf{0} & \mathbf{Q}_B^{1/2} \end{bmatrix} \mathcal{R}_{\mathrm{S}} \begin{bmatrix} \mathbf{Q}_A^{-1/2} & \mathbf{0} \\ \mathbf{0} & \mathbf{Q}_B^{-1/2} \end{bmatrix} \\ &= \begin{bmatrix} \mathbf{I} & -\mathbf{N}^T \\ \mathbf{0} & \mathbf{I} \end{bmatrix} \begin{bmatrix} \mathbf{I} & \mathbf{0} \\ \mathbf{0} & -\mathbf{I} \end{bmatrix} \begin{bmatrix} \mathbf{I} & \mathbf{0} \\ -\mathbf{N} & \mathbf{I} \end{bmatrix} \begin{bmatrix} \mathbf{I}-\mathbf{M} & \mathbf{0} \\ \mathbf{0} & \mathbf{N}\mathbf{N}^T - \mathbf{I} \end{bmatrix}. \end{aligned} \tag{21}$$

For the inexact block triangular algorithm, we assume that

$$\mathbf{A} < \mathbf{Q}_A \tag{22}$$

so that the spectrum of $\mathbf{M}$ is bounded by one, as was also assumed in [3]. We can then further apply a similarity transformation to Eq. (20) as follows.

$$\begin{aligned} &\begin{bmatrix} (\mathbf{I}-\mathbf{M})^{1/2}\mathbf{Q}_A^{1/2} & \mathbf{0} \\ \mathbf{0} & \mathbf{Q}_B^{1/2} \end{bmatrix} \mathcal{R}_{\mathrm{T}} \begin{bmatrix} \mathbf{Q}_A^{-1/2}(\mathbf{I}-\mathbf{M})^{-1/2} & \mathbf{0} \\ \mathbf{0} & \mathbf{Q}_B^{-1/2} \end{bmatrix} \\ &= \begin{bmatrix} \mathbf{I} & \mathbf{0} \\ \mathbf{0} & -\mathbf{I} \end{bmatrix} \begin{bmatrix} \mathbf{I}-\mathbf{M} & -(\mathbf{I}-\mathbf{M})^{1/2}\mathbf{N}^T \\ -\mathbf{N}(\mathbf{I}-\mathbf{M})^{1/2} & \mathbf{N}\mathbf{N}^T - \mathbf{I} \end{bmatrix}. \end{aligned} \tag{23}$$

In the case of the inexact block LU algorithm, without any further condition as in the above case, we have

$$\begin{aligned}
&\begin{bmatrix} \mathbf{I} & \mathbf{N}^T \\ \mathbf{0} & \mathbf{I} \end{bmatrix} \begin{bmatrix} \mathbf{Q}_A^{1/2} & \mathbf{0} \\ \mathbf{0} & \mathbf{Q}_B^{1/2} \end{bmatrix} \mathcal{R}_{\mathrm{S}} \begin{bmatrix} \mathbf{Q}_A^{-1/2} & \mathbf{0} \\ \mathbf{0} & \mathbf{Q}_B^{-1/2} \end{bmatrix} \begin{bmatrix} \mathbf{I} & -\mathbf{N}^T \\ \mathbf{0} & \mathbf{I} \end{bmatrix} \\
&= \begin{bmatrix} \mathbf{I} & \mathbf{0} \\ \mathbf{0} & -\mathbf{I} \end{bmatrix} \begin{bmatrix} \mathbf{I} & \mathbf{0} \\ -\mathbf{N} & \mathbf{I} \end{bmatrix} \begin{bmatrix} \mathbf{I}-\mathbf{M} & \mathbf{0} \\ \mathbf{0} & \mathbf{N}\mathbf{N}^T-\mathbf{I} \end{bmatrix} \begin{bmatrix} \mathbf{I} & -\mathbf{N}^T \\ \mathbf{0} & \mathbf{I} \end{bmatrix} \\
&= \begin{bmatrix} \mathbf{I} & \mathbf{0} \\ \mathbf{0} & -\mathbf{I} \end{bmatrix} \begin{bmatrix} \mathbf{I}-\mathbf{M} & -(\mathbf{I}-\mathbf{M})\mathbf{N}^T \\ -\mathbf{N}(\mathbf{I}-\mathbf{M}) & \mathbf{N}(2\mathbf{I}-\mathbf{M})\mathbf{N}^T-\mathbf{I} \end{bmatrix}.
\end{aligned} \tag{24}$$

Note that the matrices:

$$\widetilde{\mathcal{R}}_{\mathrm{T},1} = \begin{bmatrix} \mathbf{I}-\mathbf{M} & -(\mathbf{I}-\mathbf{M})^{1/2}\mathbf{N}^T \\ -\mathbf{N}(\mathbf{I}-\mathbf{M})^{1/2} & \mathbf{N}\mathbf{N}^T-\mathbf{I} \end{bmatrix} \tag{25}$$

$$\widetilde{\mathcal{R}}_{\mathrm{S},1} = \begin{bmatrix} \mathbf{I}-\mathbf{M} & -(\mathbf{I}-\mathbf{M})\mathbf{N}^T \\ -\mathbf{N}(\mathbf{I}-\mathbf{M}) & \mathbf{N}(2\mathbf{I}-\mathbf{M})\mathbf{N}^T-\mathbf{I} \end{bmatrix} \tag{26}$$

on the right hand sides, respectively, of Eqs. (24) and (23) are symmetric. Thus, it is easier for the error reduction analysis to work with the matrices obtained after the similarity transformation:

$$\begin{bmatrix} \widetilde{E}_i^X \\ \widetilde{E}_i^Y \end{bmatrix} = \mathcal{T} \begin{bmatrix} E_i^X \\ E_i^Y \end{bmatrix}. \tag{27}$$

Here, the transformation $\mathcal{T}$ is defined by

$$\mathcal{T} = \mathcal{T}_{\mathrm{T}} = \begin{bmatrix} (\mathbf{I}-\mathbf{M})^{1/2}\mathbf{Q}_A^{1/2} & \mathbf{0} \\ \mathbf{0} & \mathbf{Q}_B^{1/2} \end{bmatrix} \tag{28}$$

for the inexact block triangular algorithm, and

$$\mathcal{T} = \mathcal{T}_{\mathrm{S}} = \begin{bmatrix} \mathbf{I} & \mathbf{N}^T \\ \mathbf{0} & \mathbf{I} \end{bmatrix} \begin{bmatrix} \mathbf{Q}_A^{1/2} & \mathbf{0} \\ \mathbf{0} & \mathbf{Q}_B^{1/2} \end{bmatrix} \tag{29}$$

for the inexact block LU algorithm. Then, Eqs. (23) and (24) are represented as

$$\mathcal{T}\mathcal{R}\mathcal{T}^{-1} = \widetilde{\mathcal{E}}\widetilde{\mathcal{R}}_1$$

with $\widetilde{\mathcal{R}}_1 = \widetilde{\mathcal{R}}_{\mathrm{T},1}$ in Eq. (25) for the inexact block triangular algorithm, and with $\widetilde{\mathcal{R}}_1 = \widetilde{\mathcal{R}}_{\mathrm{S},1}$ in Eq. (26) for the inexact block LU algorithm, and

$$\widetilde{\mathcal{E}} = \begin{bmatrix} \mathbf{I} & \mathbf{0} \\ \mathbf{0} & -\mathbf{I} \end{bmatrix}. \tag{30}$$

Thus, the error reduction in Eq. (15) can be rewritten as

$$\begin{bmatrix} \widetilde{E}_{i+1}^X \\ \widetilde{E}_{i+1}^Y \end{bmatrix} = \widetilde{\mathcal{E}}\widetilde{\mathcal{R}}_1 \begin{bmatrix} \widetilde{E}_i^X \\ \widetilde{E}_i^Y \end{bmatrix} = \widetilde{\mathcal{R}} \begin{bmatrix} \widetilde{E}_i^X \\ \widetilde{E}_i^Y \end{bmatrix}$$

Since $\widetilde{\mathcal{E}}$ is unitary and $\widetilde{\mathcal{R}}_1$ is symmetric, the operator norm of $\widetilde{\mathcal{R}}$ is determined by the spectrum $\lambda(\widetilde{\mathcal{R}}_1)$ as

$$\|\widetilde{\mathcal{R}}\|_2{}^2 = \sup_{\widetilde{x}} \frac{(\widetilde{\mathcal{R}}\widetilde{x}, \widetilde{\mathcal{R}}\widetilde{x})}{(\widetilde{x}, \widetilde{x})} = \sup_{\widetilde{x}} \frac{(\widetilde{\mathcal{E}}\widetilde{\mathcal{R}}_1\widetilde{x}, \widetilde{\mathcal{E}}\widetilde{\mathcal{R}}_1\widetilde{x})}{(\widetilde{x}, \widetilde{x})} = \sup_{\widetilde{x}} \frac{(\widetilde{\mathcal{R}}_1\widetilde{x}, \widetilde{\mathcal{R}}_1\widetilde{x})}{(\widetilde{x}, \widetilde{x})} = \sup_{\lambda_i \in \lambda(\widetilde{\mathcal{R}}_1)} |\lambda_i|^2.$$

Thus, in the following we estimate the lower and upper bounds of spectrum $\lambda(\widetilde{\mathcal{R}}_1)$.

Lemma 1 *The inexact block triangular case:*
Suppose the condition

$$\overline{m} < 1 \tag{31}$$

is satisfied. Then, we have the following lower and upper bounds of the spectrum of $\widetilde{\mathcal{R}}_{\mathrm{T},1}$.

$$\inf_{\lambda_i \in \lambda(\widetilde{\mathcal{R}}_{\mathrm{T},1})} \lambda_i \geq -1 + \frac{1}{2}\underline{m}\,\underline{n_m}, \tag{32}$$

$$\sup_{\lambda_i \in \lambda(\widetilde{\mathcal{R}}_{\mathrm{T},1})} \lambda_i \leq 1 - \frac{1}{2}\underline{m}(2 - \overline{n_m}). \tag{33}$$

Proof First, we derive the lower bound. From the Schwarz inequality, we see that the following inequality holds for any positive number α and any vectors V, W in the first and second blocks, respectively.

$$\begin{aligned} |(V, (\mathbf{I}-\mathbf{M})^{1/2}\mathbf{N}^T W) + (W, \mathbf{N}(I-\mathbf{M})^{1/2}V)| &= 2|((\mathbf{I}-\mathbf{M})^{1/2}V, \mathbf{N}^T W)| \\ &\leq \frac{1}{\alpha}(V, (\mathbf{I}-\mathbf{M})V) + \alpha(W, \mathbf{N}\mathbf{N}^T W). \end{aligned}$$

Thus, we obtain

$$\widetilde{\mathcal{R}}_{\mathrm{T},1} \geq \begin{bmatrix} (1-\frac{1}{\alpha})(\mathbf{I}-\mathbf{M}) & \mathbf{0} \\ \mathbf{0} & (1-\alpha)\mathbf{N}\mathbf{N}^T - \mathbf{I} \end{bmatrix}.$$

In particular, by taking $\alpha = 1/2$, we obtain

$$\widetilde{\mathcal{R}}_{\mathrm{T},1} \geq \begin{bmatrix} -(\mathbf{I}-\mathbf{M}) & \mathbf{0} \\ \mathbf{0} & \frac{1}{2}\mathbf{N}\mathbf{N}^T - \mathbf{I} \end{bmatrix}.$$

For the second diagonal block, we have

$$(W, \mathbf{N}\mathbf{N}^T W) = (\mathbf{M}^{-1/2}\mathbf{N}^T W, \mathbf{M}\mathbf{M}^{-1/2}\mathbf{N}^T W) \geq \underline{m}(\mathbf{M}^{-1/2}\mathbf{N}^T W, \mathbf{M}^{-1/2}\mathbf{N}^T W)$$
$$= \underline{m}(W, \mathbf{N}\mathbf{M}^{-1}\mathbf{N}^T W) \geq \underline{m}\,\underline{n_m}(W, W).$$

This leads to Eq. (32).

Next, to obtain the upper bound in Eq. (33), we again apply the Schwarz inequality as follows.

$$|(V, (\mathbf{I}-\mathbf{M})^{1/2}\mathbf{N}^T W) + (W, \mathbf{N}(I-\mathbf{M})^{1/2}V)| = 2|((\mathbf{I}-\mathbf{M})^{1/2}V, \mathbf{N}^T W)|$$
$$\leq \alpha(\mathbf{M}^{1/2}V, \mathbf{M}^{1/2}V) + \frac{1}{\alpha}((\mathbf{I}-\mathbf{M})^{1/2}\mathbf{M}^{-1/2}\mathbf{N}^T W, (\mathbf{I}-\mathbf{M})^{1/2}\mathbf{M}^{-1/2}\mathbf{N}^T W)$$
$$= \alpha(V, \mathbf{M}V) + \frac{1}{\alpha}(W, \mathbf{N}\mathbf{M}^{-1/2}(\mathbf{I}-\mathbf{M})\mathbf{M}^{-1/2}\mathbf{N}^T W).$$

Thus, we obtain

$$\widetilde{\mathcal{R}}_{\mathrm{T},1} \leq \begin{bmatrix} \mathbf{I}-(1-\alpha)\mathbf{M} & \mathbf{0} \\ \mathbf{0} & -\mathbf{I}+\frac{1}{\alpha}\mathbf{N}\mathbf{M}^{-1/2}(\mathbf{I}-(1-\alpha)\mathbf{M})\mathbf{M}^{-1/2}\mathbf{N}^T \end{bmatrix}.$$

By substituting $\alpha = \overline{n_m}/2$, the first diagonal block on the right hand side is bounded as

$$\mathbf{I}-(1-\alpha)\mathbf{M} \leq \mathbf{I}-\frac{1}{2}(2-\overline{n_m})\mathbf{M} \leq \mathbf{I}-\frac{1}{2}\underline{m}(2-\overline{n_m})\mathbf{I}, \tag{34}$$

while the second diagonal block is bounded as

$$-\mathbf{I}+\frac{1}{\alpha}\mathbf{N}\mathbf{M}^{-1/2}(\mathbf{I}-(1-\alpha)\mathbf{M})\mathbf{M}^{-1/2}\mathbf{N}^T \leq -\mathbf{I}+\frac{1-(1-\alpha)\underline{m}}{\alpha}\mathbf{N}\mathbf{M}^{-1}\mathbf{N}^T$$
$$\leq \left(-1+\frac{1-(1-\alpha)\underline{m}}{\alpha}\overline{n_m}\right)\mathbf{I} = \left(1-2\underline{m}\left(1-\frac{\overline{n_m}}{2}\right)\right)\mathbf{I}. \tag{35}$$

From Eqs. (34) and (35), the upper bound is obtained. □

Lemma 2 *The inexact block LU case:*

Suppose that the upper bound of the spectrum of $\mathbf{M}$ *satisfies*

$$\overline{m} < \frac{3}{2}, \ i.e.\ \mathbf{A} < \frac{3}{2}\mathbf{Q}_A. \tag{36}$$

Then, we have the lower bound of the spectrum of $\widetilde{\mathcal{R}}_{\mathrm{S},1}$ *as*

$$\inf_{\lambda_i \in \lambda(\widetilde{\mathcal{R}}_{\mathrm{S},1})} \lambda_i \geq -1+\frac{3}{4}\min(\underline{m}, 3/2-\overline{m})\underline{n_m}. \tag{37}$$

Furthermore, without assuming Eq. (36), we have the upper bound as

$$\sup_{\lambda_i \in \lambda(\widetilde{\mathcal{R}}_{\mathrm{S},1})} \lambda_i \leq 1 - \frac{1}{2}\min(\underline{m}, 2-\overline{m})(2-\overline{n_m}). \tag{38}$$

Proof First, we derive the lower bound. From the Schwarz inequality, we see that the following inequality holds for any positive number α and any vectors V, W on the first and second blocks, respectively.

$$\begin{aligned}|(V, (\mathbf{I}-\mathbf{M})\mathbf{N}^T W) + (W, \mathbf{N}(I-\mathbf{M})V)| &= 2|((\mathbf{I}-\mathbf{M})V, \mathbf{N}^T W)| \\ &\leq \frac{1}{\alpha}(V, (\mathbf{I}-\mathbf{M})^2 V) + \alpha(W, \mathbf{N}\mathbf{N}^T W).\end{aligned}$$

Thus, we obtain

$$\widetilde{\mathcal{R}}_{\mathrm{S},1} \geq \begin{bmatrix} \mathbf{I}-\mathbf{M}-\frac{1}{\alpha}(\mathbf{I}-\mathbf{M})^2 & \mathbf{0} \\ \mathbf{0} & \mathbf{N}((2-\alpha)\mathbf{I}-\mathbf{M})\mathbf{N}^T - \mathbf{I} \end{bmatrix}.$$

In particular, by taking $\alpha = 1/2$, we obtain

$$\widetilde{\mathcal{R}}_{\mathrm{S},1} \geq \begin{bmatrix} -\mathbf{I}+3\mathbf{M}-2\mathbf{M}^2 & \mathbf{0} \\ \mathbf{0} & \mathbf{N}(\frac{3}{2}\mathbf{I}-\mathbf{M})\mathbf{N}^T - \mathbf{I} \end{bmatrix}.$$

The first diagonal block is bounded as

$$-\mathbf{I}+3\mathbf{M}-2\mathbf{M}^2 \geq -\mathbf{I} + \inf_{m\in[\underline{m},\overline{m}]}(3m-2m^2)\mathbf{I} \geq -\mathbf{I} + \frac{3}{2}\min\left(\underline{m}, \frac{3}{2}-\overline{m}\right)\mathbf{I}.$$

The second diagonal block is bounded as

$$\begin{aligned}\mathbf{N}\left(\frac{3}{2}\mathbf{I}-\mathbf{M}\right)\mathbf{N}^T - \mathbf{I} &\geq \mathbf{N}\mathbf{M}^{-1/2}\left(\frac{3}{2}\mathbf{M}-\mathbf{M}^2\right)\mathbf{M}^{-1/2}\mathbf{N}^T - \mathbf{I} \\ &\geq -\mathbf{I} + \underline{n_m}\inf_{m\in[\underline{m},\overline{m}]}\mathbf{I}\left(\frac{3}{2}m-m^2\right)\mathbf{I} \geq -\mathbf{I} \\ &\quad + \frac{3}{4}\min\left(\underline{m}, \frac{3}{2}-\overline{m}\right)\underline{n_m}\mathbf{I}.\end{aligned}$$

This leads to Eq. (37).

Next, the upper bound is obtained as follows. From the Schwarz inequality, we see that the following inequality holds for any positive number α and any vectors V, W